Structural determination of Yb single-crystal films grown on W(110) using photoelectron diffraction

M. E. Dávila,[1,2] S. L. Molodtsov,[3] C. Laubschat,[3] and M. C. Asensio[1,2]

[1]*Instituto de Ciencia de Materiales de Madrid (CSIC), 28049 Cantoblanco, Madrid, Spain*
[2]*LURE, Bât. 209D, Université Paris-Sud, BP34,91898 Orsay, France*
[3]*Institut für Oberflächenphysik und Mikrostrukturphysik, TU Dresden, D-01062 Dresden, Germany*

A quantitative analysis of the surface relaxation at the Yb(111) single-crystal films grown on W(110) has been undertaken applying energy-scan photoelectron diffraction technique using the two shifted components, i.e., surface and bulk of the lanthanide $4f$ core levels. Additional polar scans were recorded for a fixed photon energy along the crystal high-symmetry directions. The analysis of the data set following a trial and error fitting procedure confirmed a consistent fcc structure for all noncontaminated evaporated Yb films with the bulk lattice parameter corresponding to a value of $a = (5.44 \pm 0.05)$ Å, about 1% contracted respect to the bulk fcc Yb metal. A refinement of the structural analysis indicates an inward surface relaxation of the interlayer spacing for the first two top layers with respect to the bulk lattice parameter.

I. INTRODUCTION

Rare-earth (RE) materials have always attracted considerable interest due to their unusual magnetic and electronic properties which are related to their open $4f$ shell.[1,2] Due to their localized character, the $4f$ electrons do not contribute directly to chemical bonding. However, they lead to exotic phenomena like mixed-valence or heavy-fermion behavior. On the other hand, $4f$ electrons carry strong magnetic moments that are coupled via indirect exchange with valence electrons leading to a variety of ordered magnetic structures. These properties make RE systems interesting for applications such as hard magnets and magnetic storage materials.

Surface and interface phenomena become important for applications of RE's in the form of thin films and multilayers, because they affect the magnetic and electronic properties of the materials. Strongest effects occur when valence transitions appear at the surfaces of several Ce-, Sm-, Eu-, Tm-, and Yb-based compounds[3,4] as well as at the surfaces of the pure metals Ce,[5] Sm,[6] and Tm.[7] Surface valence-band features are characterized by an increase of the $4f$ occupation of the outermost surface atoms that results in radical changes of the chemical and magnetic properties of the surfaces. Another phenomenon that leads to an effective reduction of surface valence is due to the dehybridization of d states that appear at the close-packed surfaces of trivalent RE metals. Here, a weakly dispersive surface state of d_{z^2} symmetry lies energetically close to the Fermi energy (E_F) and extends over almost the whole surface Brillouin zone.[5,8–14] At the ferromagnetic Gd(0001) surface this state is half filled and strongly spin polarized.[11] For the paramagnetic phases of all other trivalent RE's, a comparable occupation of the corresponding surface states is observed.[5,12] In contrast to the bulk electron structure, where occupied d states are bonding and mainly responsible for the high cohesive energy of the trivalent phase, the d-like surface state is predicted to be nonbonding in nature.[8,9] For the (0001) surfaces of Gd and Tb and probably of all other trivalent RE metals, the appearance of the surface state is accompanied by an inward relax-

ation of the outermost atomic surface layer.[9,15,16] This kind of behavior of the trivalent RE metals is in contrast to the one of the trivalent sp metal Al, where an outward relaxation of the outermost atomic surface layer is observed for the close-packed (111) surface.[17] One may speculate that the surface state or at least the contribution of d states to bonding is responsible for the surface structural relaxation of the RE. In this context it is instructive to investigate the relaxational behavior of the divalent RE metal Yb, where hints for the beginning of the d-like surface state occupation have been detected.[14] Here, in analogy to the trivalent RE's an inward lattice relaxation might be expected, although the close-packed (0001) surfaces of the divalent sp metals Be and Mg reveal an outward relaxation like for Al(111).[18–20] In fact, an inward relaxation has recently been predicted for the Yb(111) surface on the basis of a structural and lattice dynamic analysis.[21] A direct experimental proof, however, is still missing.

In the present work we report on an experimental determination of the lattice parameters of epitaxial films of Yb(111) grown on W(110) by means of photoelectron diffraction (PED). The surface core-level shift (SCLS or SCS) of the Yb $4f$ states has been used to discriminate between bulk and surface signals. As compared to other structural techniques, SCS combined with PED has the advantage that due to the coordination dependence of the SCS,[22] the surface microstructure is monitored. In addition, the presence of large amounts of low coordinated sites like vacancies and terrace steps, that could influence the relaxational behavior of the surface layer, may be excluded. Furthermore, surface contaminations like oxygen or carbon that are hardly detectable in low-energy electron diffraction (LEED) become directly visible in the photoemission (PE) spectra.[23]

Scanned-energy photoelectron diffraction is a very well-known structural technique and successfully applied to study the adsorption sites of small molecules on metallic substrates.[24,25] However, the application of this technique using a SCS is still not well established.[26] It involves the measurement of the intensity of emitted photoelectrons from a core level of an atom as a function of the incident photon

energy for different emission directions. The intensity $I(k)$, where k denotes the electron wave vector, presents short-period oscillations, which are caused by diffraction effects in the final state of the photoelectrons. In this particular case high-energy-resolution photoemission spectra of the valence band have been measured and by fitting procedure of each energy-scan PED curve individual contributions of the Yb $4f$ components (surface and bulk) were obtained. Additional polar scans along the high-symmetry directions for a fixed excitation photon energy have been measured. The final purpose is to use the performance of PED to fully characterize the structure of epitaxial Yb(111) films using the separated contributions of the bulk and surface to the Yb $4f$ core-level photoemission.

In order to quantify the structural parameters, we have performed single scattering calculations followed by a trial and error procedure. This allows us to determine the optimum bulk and surface structural values of the Yb(111) films grown on W(110). In particular, we explore the bulk lattice parameter and the surface layers relaxation (outward or inward).

The paper is organized as follows. In the next section we describe the experiment. Section III presents a detailed description of the procedure followed to obtain the experimental PED curves from the raw data. The results are presented in Sec. IV and discussed in Sec. V. Finally the conclusions are summarized in Sec. VI.

II. EXPERIMENT

The measurements were carried out at LURE (Orsay, France) Synchrotron Radiation (SR) facility using the Spanish-French Station connected at the SU7 undulator beamline (toroidal grating monochromator, TGM) of the Super-Aco storage ring. The surface-science chamber was equipped with a manipulator, which allows polar and azimuthal movements with a precision of better than half a degree, and a 50-mm radius hemispherical analyzer mounted on a goniometer. The Yb(111) samples were 100-Å-thick epitaxial films grown on a W(110) single crystal. The Yb deposition was carried out at room temperature in an ambient pressure of 8×10^{-11} Torr. The films were then annealed to 465 K during 5 min resulting in clean well-ordered and atomically smooth surfaces, as verified by the sharp hexagonal LEED pattern. PE spectra of the prepared samples showed these films to be free of contaminations. Usually, possible contaminants like C and O lead to the formation of trivalent compounds, which may be easily identified by their characteristic $4f^{12}$ final-state multiplets. As compared to the $4f^{13}$ state, the $4f^{12}$ multiplet is shifted in binding energies. The spectra measured for clean samples showed two well-resolved spin-orbit split doublets corresponding to $4f$ emissions from the bulk and the surface, respectively, separated by a SCS of (0.45 ± 0.03) eV that is characteristic for a highly coordinated surface. The PED experiment was carried out by recording Yb $4f$ photoemission spectra as a function of the photon energy for different emission angles along the different crystal high-symmetry directions.
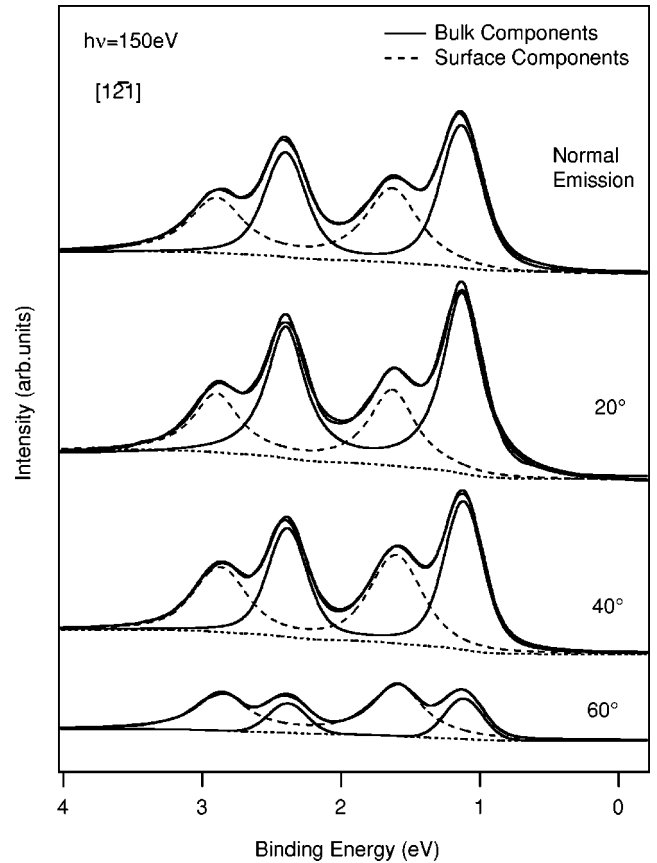
FIG. 1. Yb $4f$ core-level PE spectra of Yb(111) single-crystalline films obtained at photon energy of 150 eV and different detection geometries: normal emission (NPD) and 20°, 40°, 60° along the $[1\bar{2}1]$ high-symmetry direction (lines through data points). Individual subspectra used to fit the 150-eV spectrum are shown underneath the experimental data.

III. EVALUATION OF THE PE SPECTRA

The procedure to obtain the experimental diffraction curves was rather complicated due to the requirement to discriminate between the bulk and surface contributions and, consequently, a description of this procedure will be presented in detail in the following subsection.

A. Experimental data

In the present experiment scanned energy PED beams have been taken for the surface and bulk components of the Yb $4f^{13}$ emission at several constant emission angles in the photon energy range from 140 to 260 eV, every 2 eV. Complementary, polar scans have been performed at a fixed "surface sensitive" photon energy of 150 eV. In this way two traditionally independent modes of PED (energy and angular scans) were combined in order to determine the bulk lattice parameter and the surface lattice relaxation with an accuracy of 0.03 Å.

Figure 1 shows Yb $4f$ spectra measured at a photon energy of 150 eV for different emission angles: 0°, 20°, 40°, and 60° off normal along the $[1\bar{2}1]$ high-symmetry direction. The two peaks correspond to the $4f_{5/2}$ and $4f_{7/2}$ spin-

orbit split states. As clearly seen in the figure, the experimental Yb $4f$ spectra present two components. The higher and lower kinetic energy doublets correspond to the bulk and surface components, respectively, obtained by fitting the experimental spectra. The intensity of the surface components became larger at grazing detection angles, where photoemission spectroscopy is more surface sensitive.

In the general case each spectrum can be well decomposed into three subspectra: two Lorentzian doublets and background that consists of the steplike Fermi function superimposed by the integral scattering background from only the bulk component (dotted line). As a result of the fitting we obtain a spin-orbit split value of (1.26 ± 0.03) eV and a SCS of (0.45 ± 0.03) eV. For each set of data the values of binding energies and spin-orbit splitting were kept constant. However, variations of the intensity ratio of the $4f_{5/2}$ and $4f_{7/2}$ components were allowed. Previous publised results related that the SCS value with the bulk and the surface coordination number. For close-packed structures [hcp(0001) and/or fcc(111)],[22] the coordination number corresponds to 12 for bulk and 9 for the surface layer. The possibility of having different surface coordination numbers in our case has been neglected, because a good fit is obtained by using just one surface component. The SCS value obtained is affected by the growth conditions.[7] The SCS increases with a decreasing coordination number of surface atoms. A substantial fraction of surface atoms at low-coordinated sites will result in larger shifts than those representative for an atomically flat close-packed surface. However, this assumption can be also probed with a structural method like the PED technique.

Yb $4f$ spectra taken at different photon energies for a normal emission detection (also called normal photoelectron diffraction or NPD) and light incident angle of 30° relative to the surface plane are displayed in Fig. 2. A worsening of the energy resolution is clearly observed as the photon energy increases, reflecting the energy dependence of the resolution of the Toroidal Grating Monochromator (TGM). However, in all cases the resolution is enough to distinguish between the two components, i.e., the surface and the bulk, and to observe the drastic changes of the relative intensity of both components as the photon energy changes. In fact, we choose 260 eV as the maximum photon energy of the experiment because the surface component suffers a drastic decrease of its intensity at higher photon energies.

The branching ratio (BR) variation of the Yb $4f$ levels as a function of the photon energy has been evaluated, i.e., the relative intensity of the $4f_{7/2}$ peak respect to that of the $4f_{5/2}$ one. On the basis of statistical arguments the expected values for the BR is $(l+1)/l=1.33$. From the experimental values at photon energies of 135, 150, and 220 eV the obtained BR's were 1.33, 1.37, and 1.3 (±0.01), respectively. The photon energy dependence of the BR is a well-known effect, which is basically caused by the difference between the binding energy of the two states considered. In this particular case the two electronic states denominated $4f_{7/2}$ and $4f_{5/2}$,[27,28] with a small binding-energy difference, suffer independent diffraction effects which modify their intensity ratio.[29,30]
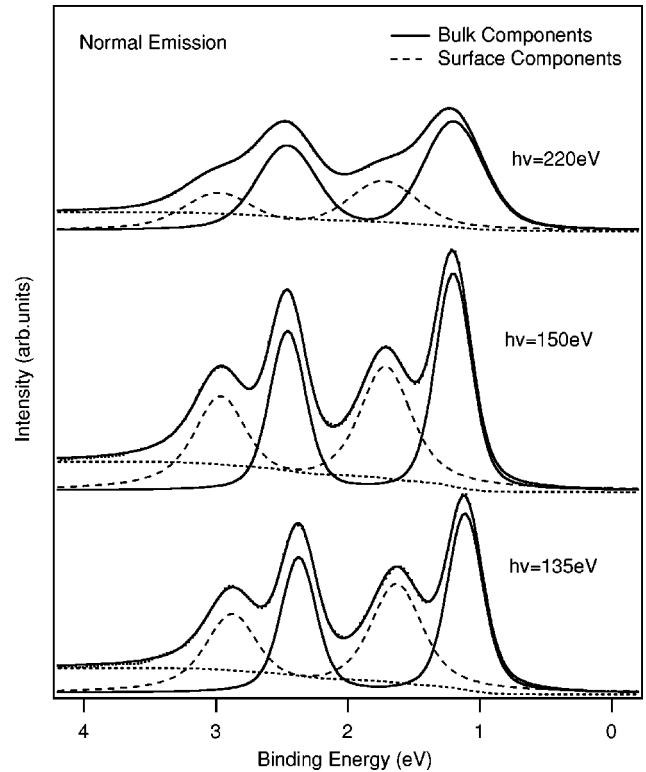
FIG. 2. Yb $4f$ core-level PE spectra of Yb(111) single-crystalline films obtained at normal emission using various photon energies: 135, 150, and 220 eV (lines through data points). Individual subspectra used to fit the different spectra are shown underneath the experimental data.

B. Obtention of the PED curves

Peaks areas after background subtraction were determined for each spectrum corresponding to each photon energy to evaluate the experimental photoelectron diffraction curves. Subsequently, these peaks were integrated and normalized to produce the modulation function $X(\mathrm{E})$ as a function of the photoelectron kinetic energy for a defined core-level peak in a specific emission direction. All intensity values were normalized to the photon flux and to the atomic $4f$ photoionization cross sections.[31] In particular, the modulation function is thus

$$X(E_{kin})=[I(E_{kin})-I_0(E_{kin})]/I_0(E_{kin})$$

in which $I(E_{kin})$ are the actual recorded peak areas, and $I_0(E_{kin})$ is the smooth fit through the average background.

Figure 3 represents normalized intensities derived from the $4f_{5/2}$ and $4f_{7/2}$ peaks at 20° off normal along the $[\bar{1}2\bar{1}]$ direction. We found that electrons photoemitted from the $4f_{5/2}$ level undergo practically the same diffraction effects as those emitted from the $4f_{7/2}$ one, since the kinetic energies of them are close to each other. The different assumptions considered in the data evaluation are now disscused: The line shape was approximated by a Lorentzian. This procedure is justified since Yb is a semimetal and only weak final-state electron-electron interactions are expected. Energy losses for the photoexcited electrons on their way through the sample
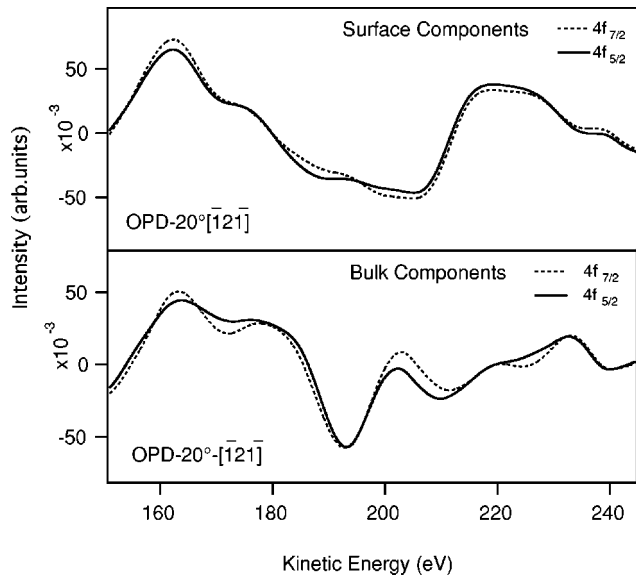
FIG. 3. Surface and bulk $4f_{7/2}$ and $4f_{5/2}$ PED patterns from Yb(111) single-crystalline films taken for 20° off-normal emission (OPD-20°) in the $[\bar{1}2\bar{1}]$ direction. All intensity values were normalized to photon flux and to the atomic $4f$ photoionization cross sections (Ref. 31). It can be seen that spin-orbit split components undergo almost same diffraction effects.

were considered only for the bulk emission and were described by an integral background. The spin-orbit splitting of the $j=7/2$ and $j=5/2$ components was set to be identical for the bulk and the surface emissions. In order to simulate the finite resolution of the spectrometer and the temperature-dependent phonon broadening, the theoretical spectra were convoluted with a Gaussian of variable width. The spectra show the $f_{5/2}$ and $f_{7/2}$ spin-orbit doublet, where the surface lines are shifted to larger binding energies. The surface contribution can be directly recognized by comparing data taken with two different photon energies. At the higher photon energy, the escape depth is increased and the surface contribution is correspondingly reduced. Surface core-level shifts are rather small. Thus for their detection one needs high resolution, which is most easily achieved with synchrotron radiation. The tunability of the SR photon source also makes it possible to perform measurements at different surface sensitivity.

As a result of data evaluation the intensity curves for the $4f_{7/2}$ and $4f_{5/2}$ components of both bulk and surface emissions were obtained as a function of photon (kinetic) energy and emission angle. The relative intensity extracted by fitting bulk and surface emissions of $4f_{7/2}$ and $4f_{5/2}$ peaks shows the characteristic oscillations produced by the photodiffraction phenomenon. The drastic intensity variation of the two emissions as photon energy increases limited the energy range of investigation. In particular, the surface component is characterized by a strong decrease of its emission at high photon energies.

The photoelectron kinetic energy dependence is affected by the photoionization cross section of the corresponding level. Having extracted the energy dependence due to the photoionization cross section, the characteristic oscillations
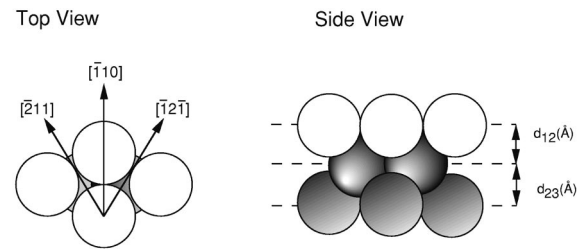
FIG. 4. Top and side views of Yb(111). Crystal directions and coordinate axes are shown. d_{12} represents the interlayer distance from the top to the second layer and d_{23}, from the second to the third layer, respectively.

produced by the photoelectron diffraction phenomenon appear with their genuine magnitude. Strong intensity modulations of the bulk and surface components were observed at certain detection geometries, in which emitter, scatter, and detector were aligned. Finally, the diffraction curves for the different geometries were obtained for the two surface and bulk Yb $4f$ components following the standard procedure.

IV. QUANTITATIVE DETERMINATION OF THE BULK AND SURFACE ATOMIC STRUCTURE

The structural parameters for the fcc(111) and hcp(0001) tested structures were adjusted in order to minimize a reliability factor (R factor) between single-scattering simulations and the experimental diffraction curves. This R factor is based on a sum of squared deviations between theory and experiment of a representative number of PED curves for different emission directions. In the adjustment process the correlation or anticorrelation evaluation, the PED curves with small modulations contribute less than curves with strong modulations.

Experimental energy scan curves for defined geometries and complementary low-energy polar scans for high-symmetry directions were considered following the traditional trial and error procedure data analysis. The fitting procedure was performed by the calculation of multiple parameter grids. The nonstructural parameters used in the simulations to determine the final structure were defined as follows: The energy-dependent phase shifts used to describe the elastic scattering of the electrons by the surface atoms were calculated with the MUFPOT program.[32] In addition, different constants and the Debye factor were adjusted in order to optimize the fitting of the experimental data.

Since photoelectron diffraction is sensitive to the local geometry structure around the emitter, we may need to find the lattice parameter of the bulk atoms from the bulk components and to evaluate the possible deviations from the ideal surface interlayer spacing from the surface component. Based on this criteria the analysis was divided into two steps: First of all, both the fcc(111) (Fig. 4) and the hcp(0001) structures were considered because both arrangements are plausible with the experimental SCS values obtained in the studied Yb films. We have calculated the PED curves for each of these structures considering the corresponding bulk lattice parameter (fcc $a=5.49$ Å, hcp $a=3.88$ Å, and c
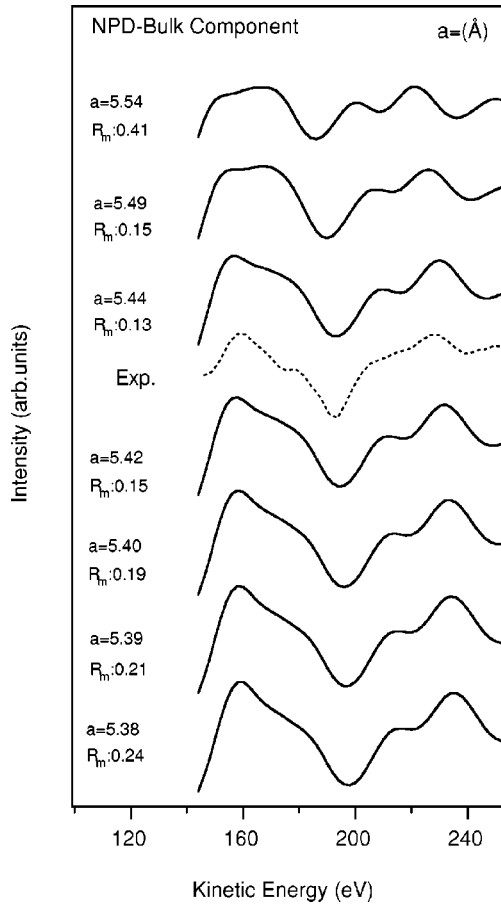
FIG. 5. Theory-experiment curves comparison of the corresponding bulk component at normal emission geometry considering different bulk lattice parameters. Best agreement is obtained for a lattice constant value of $a = (5.44 \pm 0.05)$ Å.

FIG. 6. R-factor image contour plot calculated varying the Yb interlayer spacing d_{12} and d_{23}. Best agreement is obtained for inward relaxation differences of $\Delta d_{12} = -0.1$ Å and $\Delta d_{23} = -0.06$ Å relative to the bulk interlayer spacing.

$= 6.20$ Å).[33] From the comparison between the experimental and the calculated curves we have obtained an extended correlation, which ensure the fcc(111) as the authentic structure. Using the bulk PED curves the bulk lattice parameter was refined. Various clusters with different bulk lattice constants were considered, as represented for NPD bulk spectra in Fig. 5.

From the theory-experiment comparison we conclude that a value of the bulk lattice constant $a = (5.44 \pm 0.05)$ Å is obtained, revealing that the lattice spacing is the same as the bulk value within 1%. As mentioned before, only small changes are obtained in the diffraction effects between the two bulk components with different j (same behavior is observed for the two surface components).

In a second step the surface layer relaxation is studied by analyzing the surface PED curves. A multiple parameter grid has been calculated and represented in Fig. 6 as an image contour map of the R factor as a function of the different interlayer spacing for the first (Δd_{12}) and second (Δd_{23}) surface layers relative to bulk interlayer spacing. This contour plot tests the sensitivity of the experimental data to the surface relaxation. From the figure the correlation between the two represented parameters (Δd_{12} and Δd_{23}) can be deduced. As a consequence, changes in the first to second layer

distance with respect to bulk induce also proportional changes in the interlayer spacing of the second to third layer, as seen in the R factor plot. The R-factor value is consistently 0.25 indicating a good agreement between theory and experiment.

Comparison between experimental and theoretical diffraction curves at the R-factor minimum position is presented in Fig. 7. The relevant structures of the experimental curves in the figure are well reproduced by the calculations. The optimal structural parameters are summarized in Table I and compared with relatively recent theoretical predictions.[21] Inward relaxations of the first and second surface layers are $\Delta d_{12} = -0.1$ Å and $\Delta d_{23} = -0.06$ Å, i.e., $(3.6 \pm 0.3)\%$ and $(1.9 \pm 0.2)\%$, respectively. The obtained relaxation value of the outermost atomic surface layer (close to the limit of the technique resolution) is of the same order of magnitude as the values measured for the trivalent RE metals and even larger than the value of 0.08% predicted by the semiempirical calculations.[21] Further analysis relative to deeper layers, i.e., third to fourth layer was not performed in the present study. These results have been tested by the use of multiple-scattering calculations in order to evaluate the contribution of multiple events in the photodiffraction modulation. In particular, calculations using van Hove's code confirm the results presented in this report.

V. DISCUSSION

The possibility of getting individual information from the surface and the bulk components was carried out due to the relatively large SCS value for the Yb system. The SCS has been explained in a number of ways, its origin ultimately lies in the modification of the surface structure with respect to the bulk structural environment. In rare earths, the SCS leads to an increase of the $4f$ binding energy at the surface relative
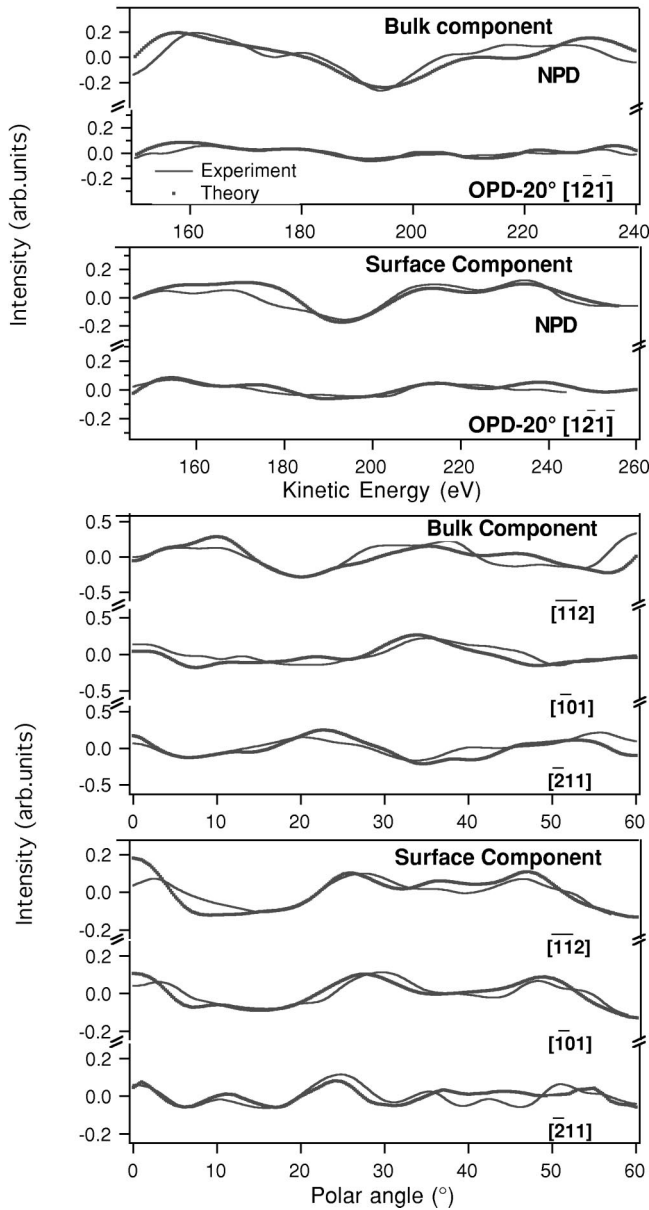
FIG. 7. Comparison of surface and bulk $4f_{7/2}$ PED patterns from Yb(111) single-crystalline films. All intensity values were normalized to photon flux. In the case of energy scans measured in normal emission (NPD) and 20° off-normal emission (OPD-20°-[$\bar{1}2\bar{1}$] direction) geometries the obtained intensities were also normalized to the atomic $4f$ photoionization cross sections (Ref. 31). For angular scans a $\cos^2(\phi)$ dependence of the photoemission intensity, where the angle ϕ is formed by the electric field vector of the linearly polarized synchrotron radiation and the direction of the electron detection, was assumed.

to the bulk, and in certain cases even to a valence transition. Changes of the SCS of Yb samples can also be due to possible contaminants.

It is of relevance to emphasize that $4f$ electrons are core-level-like while the $5d$ and $6s$ valence electrons take part in bonding the Yb metal. The energies of the $4f^n(5d6s)^2$ and of $4f^{n-1}(5d6s)^3$ configurations are sufficiently close to each other so that fluctuations between the two valence states

TABLE I. Percentage relaxations obtained in the present PED experiment and comparison with theoretical predictions (Ref. 21). Negative values correspond to inward relaxation in interlayer spacing compared to those in the bulk.

	This work	H Cox *et al.* (Ref. 20)
$\Delta d_{12}(\%)$	-3.6	-0.08
$\Delta d_{23}(\%)$	-1.9	0.06
$\Delta d_{34}(\%)$	not considered	-0.07

can occur. The energetic proximity of these configurations depends on the number, distance, and nature of the neighbors of the rare-earth cores, which can be changed by pressure, temperature, or compound formation and by changing the dimensionality of the system. Coordination dependent SCS has been observed for Yb metal evaporated samples onto substrates at different temperatures.[22] SCS has found widespread applications in probing surface electronic structure, surface structure, and surface segregation phenomena.[3,34,35]

From the present study an inward surface lattice relaxation has been confirmed. This phenomenon can be correlated with different effects. The surface relaxation in alkali metals, particularly effective for low-coordinated surfaces,[36-38] is related with the variations of charge density by the electron spill out at the surface. Changes of the electron density results in a dipole surface layer. The positive ion cores at the surface are affected by a net repulsion from the resulting charge in their Wigner-Seitz cells, and an inward relaxation can occur. Other possible mechanisms such as the rehybridization of dangling bonds also lead to a surface inward relaxation.

The relaxation effect, however, becomes rather small at close-packed surfaces. A relaxation by only 1% of the lattice constant has been observed on (bcc) Na (100),[36,37] and even smaller values are expected for the close-packed (111) surfaces of fcc crystals, which may be easily compensated by other effects. Weakening of the bonding due to a surface dehybridization of s and p states is present in Be and Mg metals, and it is assumed of being responsible for the outward relaxation of the outermost atomic layers here.[18,19] Although in the present case of Yb metal, the sp hybridization is widely replaced by the sd hybridization, similar dehybridization effects may be expected by narrowing of the $5d$ bands at the surface.

Dehybridization at the Yb(111) surface leads to a formation of a d-like surface state, which becomes partly occupied around the $\bar{\Gamma}$ point of the surface Brillouin zone.[14] The charge-density distribution related with such a surface state may cause an enhancement of the effective electronic spill out and may be responsible for the inward relaxation observed in the present work. On the other hand, changes of the surface dipole layer should directly affect the work function. To this end, however, results of slab calculations, which do not reproduce the occupied surface state, are in reasonable agreement with the experiment[14] indicating that the change of the surface dipole layer by the presence of the surface state is only small. From this fact one might conclude that a

possible influence of the surface state is also too weak to affect the surface relaxation.

The second mechanism to explain the inward relaxation of Yb (111) considers an enhancement of the bonding strength due to rehybridization of dangling bonds. This mechanism is responsible for the large inward relaxations (about 5–10%) of the lattice constant observed in transition metals. From recent local density approximation and linear combination of atomic orbitals electron-structure calculations for bulk Yb metal (detailed in Ref. 14), the $5d$ admixtures to the occupied density of states near the Fermi level can be estimated as only 0.27 electrons per Yb atom and therefore contributes weakly to the bonding. At the surface, the d occupation may be changed due to the presence of the surface state. In analogy to the case of trivalent RE's, however, the surface state will be nonbonding and an increase of bonding strength at the surface is not expected.

From this analysis it seems that the charge distribution may be responsible for the inward relaxation and not the bonding properties of the surface.

VI. CONCLUSIONS

In summary, we have presented a structural analysis of the Yb(111) films grown *in situ* on W(110) substrates by using the PED technique. Due to the observed relatively large SCS independent interpretation of the surface and bulk Yb $4f$ components are presented. Yb films are subject to an inward relaxation that amounts to $(3.6\pm0.3)\%$ and $(1.9\pm0.2)\%$ of the bulk interlayer spacing for the first and second surface atomic layers, respectively. For the outermost surface layer this result is in qualitative agreement with theoretical predictions based on an analysis of lattice dynamic data.[21] This behavior is opposite, however, to the properties of the divalent sp metals Be and Mg, where an outward relaxation of the outermost close-packed surface layer has been reported. The Yb(111) surface relaxation is similar to those observed for trivalent RE's. A possible explanation for this surface relaxation is based on surface charge distribution that in both cases is governed by a partially occupied surface state.

[1] For a complete overview, the reader is referred to the series *Handbook on Physics and Chemistry of Rare-Earths* (North-Holland, Amsterdam, Vols. 1–31, 1978–2001).

[2] P. Strange, A. Svane, W. M. Temmerman, Z. Szotek, and H. Winter, Nature (London) **399**, 756 (1999).

[3] C. Laubschat, G. Kaindl, W. D. Schneider, B. Reihl, and N. Martensson, Phys. Rev. B **33**, 6675 (1986).

[4] C. Laubschat, E. Weschke, C. Holtz, M. Domke, O. Strebel, and G. Kaindl, Phys. Rev. Lett. **65**, 1639 (1990).

[5] E. Weschke, A. Hohr, G. Kaindl, S. L. Molodtsov, S. Danzenbacher, M. Richter, and C. Laubschat, Phys. Rev. B **58**, 3682 (1998).

[6] G. K. Wertheim and G. Crecelius, Phys. Rev. Lett. **40**, 813 (1978).

[7] M. Domke, C. Laubschat, M. Prietsch, T. Mandel, G. Kaindl, and W. D. Schneider, Phys. Rev. Lett. **56**, 1287 (1986).

[8] R. Wu, C. Li, A. J. Freeman, and C. L. Fu, Phys. Rev. B **44**, 9400 (1991).

[9] D. M. Bylander and L. Kleinman, Phys. Rev. B **50**, 4996 (1994).

[10] B. Kim, A. B. Andrews, J. L. Erskine, K. J. Kim, and B. N. Harmon, Phys. Rev. Lett. **68**, 1931 (1992).

[11] G. A. Mulhollan, K. Garrison, and J. L. Erskine, Phys. Rev. Lett. **69**, 3240 (1992).

[12] G. Kaindl, A. Hohr, E. Weschke, S. Vandre, C. Schussler-Langeheine, and C. Laubschat, Phys. Rev. B **51**, 7920 (1995).

[13] A. V. Fedorov, C. Laubschat, K. Starke, E. Weschke, K. U. Barholz, and G. Kaindl, Phys. Rev. Lett. **70**, 1719 (1993).

[14] M. Bodenbach, A. Hohr, C. Laubschat, G. Kaindl, and M. Methfessel, Phys. Rev. B **50**, 14 446 (1994).

[15] J. Quinn, Y. S. Li, F. Jona, and D. Fort, Phys. Rev. B **46**, 9694 (1991).

[16] J. Quinn, Y. S. Li, F. Jona, and D. Fort, Surf. Sci. Lett. **257**, L647 (1991).

[17] J. R. Nooman and H. L. Davies, J. Vac. Sci. Technol. A **8**, 2671 (1990).

[18] A. F. Wright, P. J. Feibelman, and S. R. Atlas, Surf. Sci. **302**, 215 (1994); P. T. Sprunger, K. Pohl, H. L. Davis, and E. W. Plummer, Surf. Sci. Lett. **297**, L48 (1993).

[19] P. J. Feibelman, Phys. Rev. B **46**, 2532 (1992).

[20] H. L. Davis, J. B. Hannon, K. B. Ray, and E. W. Plummer, Phys. Rev. Lett. **68**, 2632 (1992); K. M. Schindler, Ph. Hofmann, V. Fritzsche, S. Bao, A. M. Bradshaw, and D. P. Wooduff, *ibid.* **71**, 2054 (1993).

[21] H. Cox, R. L. Johnston, and A. Ward, J. Phys.: Condens. Matter **10**, 9419 (1998).

[22] W. D. Schneider, C. Laubschat, and B. Reihl, Phys. Rev. B **27**, 6538 (1983).

[23] R. Meier, E. Weschke, A. Bievetski, C. Schussler-Langeheine, Z. Hu, and G. Kaindl, Chem. Phys. Lett. **292**, 507 (1998).

[24] M. E. Dávila, M. C. Asensio, D. P. Woodruff, K. M. Schindler, P. Hofmann, S. Bao, V. Fritzsche, and A. M. Bradshaw, Surf. Sci. **359**, 185 (1996).

[25] R. Dippel, D. P. Woodruff, X. M. Hu, M. C. Asensio, A. W. Robinson, K. M. Schindler, K. U. Weiss, P. Gardner, and A. M. Bradshaw, Phys. Rev. Lett. **68**, 1543 (1992).

[26] K. C. Prince, B. Ressel, C. Astaldi, M. Peloi, R. Rosei, M. Polcik, C. Crotti, M. Zacchigna, C. Comicioli, C. Ottaviani, C. Quaresima, and P. Perfetti, Surf. Sci. **377-379**, 117 (1997).

[27] T. E. H. Walker, J. Berkowitz, J. L. Dehmer, and J. T. Waber, Phys. Rev. Lett. **31**, 678 (1973); T. E. H. Walker and J. T. Waber, J. Phys. B **7**, 674 (1974).

[28] G. Margaritondo, J. E. Rowe, and S. B. Christman, Phys. Rev. B **19**, 2850 (1979).

[29] M. T. Sieger, T. Miller, and T. C. Chiang, Phys. Rev. Lett. **75**, 2043 (1995).

[30] E. L. Bullock, R. Gunnella, C. R. Natoli, H. W. Yeom, S. Kono, L. Patthey, R. I. G. Uhrberg, and L. S. O. Johansson, Surf. Sci. **352-354**, 352 (1996).

[31] J. J. Yeh and I. Lindau, At. Data Nucl. Data Tables **32**, 1 (1985).

[32] T. L. Loucks, *Augmented Plane Wave Method* (Benjamin, New York, 1967).

[33] C. Boulesteix, M. Gasgnier, Ch. H. La Blanchetais, and L. Valiergue, Thin Solid Films **5**, 15 (1970).

[34] P. J. Feibelman, Phys. Rev. B **27**, 2531 (1983).

[35] S. D. Barret, Surf. Sci. Rep. **14**, 271 (1992).

[36] K. P. Bohnen, Surf. Sci. **147**, 304 (1984).

[37] P. Blaise, J. P. Malrieu, and D. Maynau, Surf. Sci. **221**, 513 (1989).

[38] P. Jiang, P. M. Marcus, and F. Jona, Solid State Commun. **59**, 275 (1986).